Journal of Engineering Mathematics **40:** 355–376, 2001.

Numerical study of flow in a constricted curved annulus: An application to flow in a catheterised artery

G. JAYARAMAN and R. K. DASH*
Department of Mathematics, Indian Institute of Technology, Hauz Khas, New Delhi-110016, India
e-mail: jgirija@cas.iitd.ernet.in

Received 9 April 1999; accepted in revised form 19 January 2001

Abstract. The flow of an incompressible Newtonian fluid in a curved annulus with a local constriction at the outer wall is investigated numerically. The three-dimensional nonlinear elliptic partial differential equations governing the flow are simplified by use of small curvature and mild constriction approximations. The simplified equations of motion, which are locally two-dimensional elliptic in nature at each cross-section, are solved numerically by means of the finite-difference method described by Collins and Dennis [Quart. Jour. Mech. Appl. Math. 28 (1975) 133–156]. Although the results are restricted to small curvature and mild constriction, these are valid for all Dean numbers D in the entire laminar flow regime. The numerical results show that, for higher values of radii ratio k, the pressure gradient, pressure drop, and frictional resistance increase considerably and they vary markedly across the constricted length. These results are used to estimate the increase in frictional resistance in an artery when a catheter is inserted into it. *In the absence of constriction* ($\delta_1 = 0$) and depending on the value of k ranging from 0·1 to 0·7, the frictional resistance increases by a factor ranging from 1·32 to 23·91 for $D = 500$ and 1·20 to 16·56 for $D = 2000$. But, *in the presence of constriction* ($\delta_1 = 0{\cdot}1$) with the same range for k, the increase in frictional resistance is by a factor ranging from 1·34 to 42·32 for $D = 500$ and 1·18 to 29·5 for $D = 2000$. *In a straight annulus*, the increased factor ranges from 1·74 to 32·61 for $\delta_1 = 0$ and 1·78 to 58·27 for $\delta_1 = 0{\cdot}1$ (for all Dean numbers D).

Key words: blood flow, catheterised artery, constriction, curved annulus, numerical simulation.

1. Introduction

Curved pipe/duct/annular configurations are of immense practical importance in almost all piping systems, the human cardiovascular system, and in several engineering devices such as heat and mass exchangers, chemical reactors, chromatography columns, and other processing equipment. Owing to the wide range of applications, the interest in the study of flow characteristics in these configurations has grown enormously during the last few decades.

The first theoretical study on steady fully developed flow of an incompressible Newtonian fluid in a loosely coiled curved pipe was made by Dean [1, 2] for values of the Dean number D (similarity parameter) up to 96. Subsequently, there have been numerous theoretical and experimental investigations on steady, unsteady, developing, and fully developed flows in curved tubes of circular and non-circular cross-sections which are extensively reviewed by Pedley [3], Berger *et al.* [4] and Ito [5].

The numerical solution of Dean's problem for intermediate and higher values of Dean number D were obtained by McConalogue and Srivastava [6] for $96 \leq D \leq 605$, Truesdell and Alder [7] for $96 \leq D \leq 3578$, Greenspan [8], Collins and Dennis [9] and Dennis [10] for

*Present address: National Simulation Resource, Department of Bioengineering, Box 357962, University of Washington, Seattle, WA-98195, USA

$96 \leq D \leq 5000$ by using finite-difference schemes of different accuracy. The significance of the numerical solution by Collins and Dennis [9] was that it was of second-order accuracy with respect to grid sizes and it established the asymptotic structure of the solution for $D \to \infty$. The multiple solution for flow in curved pipes/ducts was obtained by Dennis and Ng [11], Daskopoulos and Lenhoff [12], Kao [13] and Mees *et al.* [14].

With an objective to understand the role of fluid mechanics on cardiovascular diseases like atherosclerosis (the disease occurs at certain preferential sites like curved portions and flow dividers of the arterial tree), several studies related to flow in curved pipes were undertaken to estimate the wall shear stress. Padmanabhan and Jayaraman [15] and Jain and Jayaraman [16] studied the flow characteristics in curved constricted tubes of circular and elliptic cross-sections, respectively, based on a double-series perturbation analysis for small curvature and mild constriction. The experimental study on flow characteristics in a curved vessel with an aneurysm was made by Niimi *et al.* [17]. The numerical simulation of pulsatile or oscillatory flow in a curved tube was made by Chang and Tarbell [18, 19] and Schilt *et al.* [20] .

Catheters attached with various functional tools have extensive use in contemporary medical science. The measurements of various physiological flow characteristics (such as arterial blood pressure or pressure gradient and flow velocity or flow rate) as well as the diagnosis and treatment of various arterial diseases (such as X-ray angiography, intravascular ultrasound, and coronary balloon angioplasty) are done through an appropriate catheter-tool device by inserting the device into a peripheral artery and positioning it in the desired part of arterial network (Sarkar and Jayaraman [21]). Recent interest in flow in curved annulus (*e.g.*, Ebadian [22], Karahalios [23], Jayaraman and Tiwari [24], and Dash *et al.* [25]) is due to their applicability to understand the changed flow pattern in a catheterised artery and to introduce corrections to the measured pressure or pressure gradient using catheters.

In our earlier paper (Dash *et al.* [25]) we studied the flow of an incompressible Newtonian fluid in a curved annulus with a local constriction at the outer wall. The mathematical analysis was based on a double-series perturbation method for small curvature and mild constriction. However, the application of the model was limited to flow situations with only moderate values of Reynolds number Re or Dean number D due to the lack of convergence of the perturbation series for higher values of Re or D.

In this paper, the flow in a curved annulus with a local constriction at the outer wall is investigated numerically. The primary objective is to extend the results of the analytic approach of Dash *et al.* [25] to larger values of Re or D. The details of the mathematical formulation, including the simplification of the governing equations of motion, are given in Section 2. The numerical schemes for the simplified equations and the computational procedure are discussed in Section 3. The effects of Dean number D and radii ratio k on various flow characteristics – *i.e.*, flow rate, pressure gradient, pressure drop, frictional resistance, friction factor, wall shear stress, and the primary and secondary flow patterns – are discussed in Section 4; the concluding remarks are given in Section 5. We have also discussed an important application of this study to a clinical problem - flow in a stenosed artery with an inserted catheter - as required to model in balloon angioplasty and during blood pressure measurements using catheters.

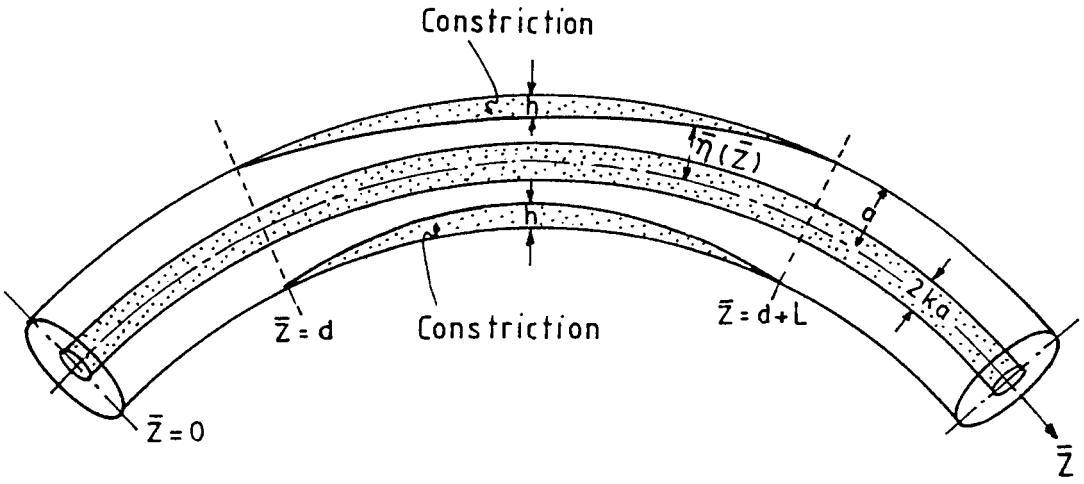

Figure 1. The schematic diagram of the flow geometry corresponding to a curved annulus with constriction.

2. Mathematical formulation

2.1. Flow geometry and co-ordinate system

Figure 1 shows the schematic diagram of the flow geometry corresponding to flow of an incompressible Newtonian fluid in an annular space between a constricted curved circular pipe of undisturbed radius a and a co-axial uniform curved circular pipe of radius ka with radii ratio $k < 1$. The annulus is coiled in the form of a circle of radius b. The variation $\overline{\eta}(\overline{z})$ of the outer wall in the constricted region $d \leq \overline{z} \leq d + L$ is assumed to have the following form

$$\frac{\overline{\eta}(\overline{z})}{a} = 1 - \frac{h}{a} \sin \pi \left(\frac{\overline{z} - d}{L} \right), \tag{1}$$

where h is the amplitude and L is the length of the constricted segment. The flow geometry is also assumed to lie in a plane, so that the effect of torsion can be neglected.

Figure 2 shows the system of toroidal co-ordinates $(\overline{r}, \theta, \phi)$ used to analyse the flow field in the geometry mentioned above. C is the centre of cross-section of the tube that makes an angle φ with the fixed axial plane and P is an arbitrary point in the cross-section whose polar co-ordinates are $(\overline{r},\ \phi)$. OC is the length b which is the radius of curvature of the curved tube. The axial co-ordinate is defined by $\overline{z} = b\phi$.

2.2. Governing equations and boundary conditions

In the co-ordinate system described above, the non-dimensional equations governing the steady flow are given by (see Pedley [3], Padmanabhan and Jayaraman [15] and Dash *et al.* [25])

$$\begin{aligned} \nabla_\delta u - \frac{v^2}{r} - \frac{\varepsilon w^2 \cos\theta}{H} = -\frac{\partial p}{\partial r} + \frac{1}{\mathrm{Re}} \Bigg[\Delta_\delta u - \frac{u}{r^2} - \frac{2}{r^2}\frac{\partial v}{\partial \theta} + \frac{\varepsilon v \sin\theta}{rH} \\ - \frac{\varepsilon \sin\theta}{rH}\frac{\partial u}{\partial \theta} + \frac{\varepsilon \cos\theta}{H}\frac{\partial u}{\partial r} - \frac{2\varepsilon\delta\cos\theta}{H^2}\frac{\partial w}{\partial z} - \frac{\varepsilon^2 u \cos^2\theta}{H^2} + \frac{\varepsilon^2 v \sin\theta\cos\theta}{H^2} \Bigg], \end{aligned} \tag{2a}$$

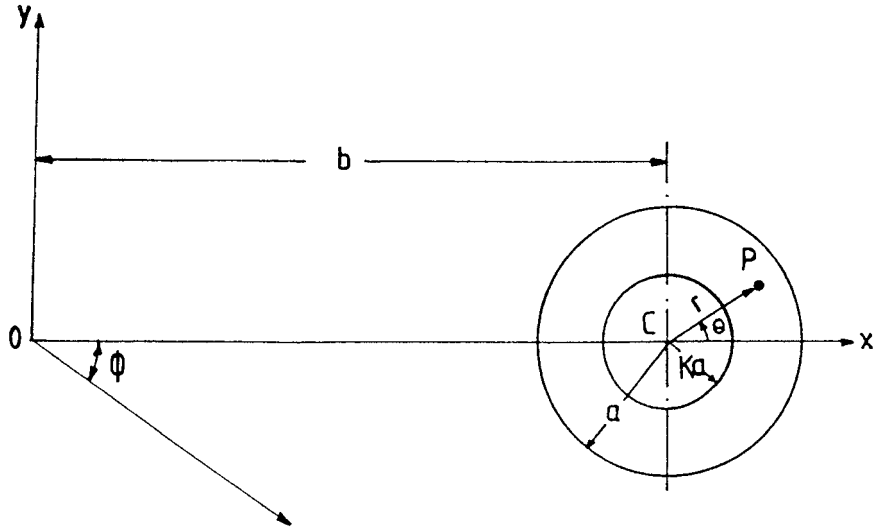

Figure 2. The toroidal co-ordinate system for the flow geometry.

$$\nabla_\delta v + \frac{uv}{r} + \frac{\varepsilon w^2 \sin\theta}{H} = -\frac{1}{r}\frac{\partial p}{\partial \theta} + \frac{1}{\mathrm{Re}}\left[\Delta_\delta v - \frac{v}{r^2} + \frac{2}{r^2}\frac{\partial u}{\partial \theta} - \frac{\varepsilon u \sin\theta}{rH} - \frac{\varepsilon \sin\theta}{rH}\frac{\partial v}{\partial \theta} + \frac{\varepsilon \cos\theta}{H}\frac{\partial v}{\partial r} + \frac{\varepsilon\delta\cos\theta}{H^2}\frac{1}{H^2}\frac{\partial w}{\partial z} - \frac{\varepsilon^2 v \sin^2\theta}{H^2} + \frac{\varepsilon^2 u \sin\theta\cos\theta}{H^2}\right], \tag{2b}$$

$$\nabla_\delta w + \frac{\varepsilon w}{H}(u\cos\theta - v\sin\theta) = -\frac{\delta}{H}\frac{\partial p}{\partial z} + \frac{1}{\mathrm{Re}}\left[\Delta_\delta w - \frac{\varepsilon^2 w}{H^2} - \frac{\varepsilon\sin\theta}{rH}\frac{\partial w}{\partial \theta} + \frac{\varepsilon\cos\theta}{H}\frac{\partial w}{\partial r} - \frac{2\varepsilon\delta\sin\theta}{H^2}\frac{\partial v}{\partial z} + \frac{2\varepsilon\delta\cos\theta}{H^2}\frac{\partial u}{\partial z}\right], \tag{2c}$$

$$\frac{\partial u}{\partial r} + \frac{u}{r} + \frac{1}{r}\frac{\partial v}{\partial \theta} + \frac{\varepsilon u\cos\theta}{H} - \frac{\varepsilon v\sin\theta}{H} + \frac{\delta}{H}\frac{\partial w}{\partial z} = 0, \tag{2d}$$

where

$$\nabla_\delta = u\frac{\partial}{\partial r} + \frac{v}{r}\frac{\partial}{\partial \theta} + \frac{\delta w}{H}\frac{\partial}{\partial z} \quad \text{and} \quad \Delta_\delta = \frac{\partial^2}{\partial r^2} + \frac{1}{r}\frac{\partial}{\partial r} + \frac{1}{r^2}\frac{\partial^2}{\partial \theta^2} + \frac{\delta^2}{H^2}\frac{\partial^2}{\partial z^2}. \tag{3}$$

Here $\mathbf{q} = (u, v, w)$ is the velocity field in (r, θ, z) co-ordinates, p is the pressure field, and $H = 1 + \varepsilon r\cos\theta$. The parameters occurring in the problem through these equations are the Reynolds number Re, the curvature parameter ε, and the geometric parameter δ defined by

$$\mathrm{Re} = \frac{\rho a U_0}{\mu}, \quad \varepsilon = \frac{a}{b}, \quad \delta = \frac{a}{L}, \tag{4}$$

where U_0 is the characteristic velocity, μ is the viscosity, and ρ is the density of the fluid. The non-dimensionalisation of various variables has been performed as follows

$$(u, v, w) = \left(\frac{\overline{u}}{U_0}, \frac{\overline{v}}{U_0}, \frac{\overline{w}}{U_0}\right), \quad p = \frac{\overline{p}}{\rho U_0^2}, \quad z = \frac{\overline{z} - d}{L}, \quad r = \frac{\overline{r}}{a}, \quad \eta = \frac{\overline{\eta}}{a}, \quad \delta_1 = \frac{h}{a}. \tag{5}$$

The appropriate boundary conditions for the problem under study are the no-slip conditions at the outer wall and the inner wall, *i.e.*,

$$u = v = w = 0 \quad \text{at} \quad r = \eta(z) \quad \text{and} \quad r = k, \tag{6}$$

where

$$\eta(z) = 1 - \delta_1 \sin \pi z \quad \text{for} \quad 0 \leq z \leq 1. \tag{7}$$

So two more parameters, *i.e.*, the radii ratio k and the constriction parameter δ_1, enter into the problem through the above boundary conditions. The other boundary condition is the symmetric condition for the flow field about the central plane (*i.e.*, the plane passing through OX and perpendicular to OY in Figure 2):

$$\frac{\partial u}{\partial \theta} = v = \frac{\partial w}{\partial \theta} = 0 \quad \text{at} \quad \theta = 0 \quad \text{and} \quad \theta = \pi. \tag{8}$$

The axial pressure gradient is obtained from the condition that the flux (flow rate) Q is independent of the axial distance z.

2.3. Simplification of the problem

The three-dimensional nonlinear elliptic partial differential equations (2a)–(2d) are not amenable to numerical solution. So, we simplify these equations through the following steps.

I. We define the characteristic velocity as $U_0 = \mu/\rho a$ so that the Reynolds number Re defined by Equation (4) becomes unity.

II. Since the centrifugal force terms drive the secondary motion, we need to rescale the velocities to make the centrifugal-force terms to be of the same order of magnitude as the viscous and inertial terms. This is accomplished through the transformation $(u, v, w) \rightarrow (u, v, (2\varepsilon)^{-1/2} w)$.

III. We assume that the radius of curvature of the outer pipe is large compared to its mean radius (*i.e.*, $\varepsilon = a/b \ll 1$) so that the terms of $O(\varepsilon)$ and higher-order terms in ε can be neglected. The effect of curvature is taken into account through the terms of $O(\varepsilon^{1/2})$. This is the loosely coiled approximation in curved-pipe flows (see Dean [1, 2], Pedley [3], and Berger *et al.* [4]).

IV. Again, we assume that the length of the constriction is very large as compared to the mean radius of the outer pipe (*i.e.*, $\delta = a/L \ll 1$) so that the terms of $O(\delta)$ and higher order terms in δ can also be neglected compared to the terms of $O(1)$. Nevertheless, the effect of constriction is taken into consideration through the no-slip boundary condition (6) at the outer wall defined by Equation (7) in the constricted region $0 \leq z \leq 1$. This is, in fact, the order of magnitude approach of Young [26] modified for the flow characteristics in a curved constricted pipe/annulus. This assumption makes the governing equations locally two-dimensional and the axial co-ordinate z appears as a parameter in the problem.

Under the above assumptions, the pressure field can be approximated by

$$p \approx \frac{1}{\delta} G f(z) + p_1(r, \theta, z), \tag{9}$$

where G is a constant and $f(z)$ is an unknown function to be determined by using the constant flux condition; $f(z) = z$ when $\delta_1 = 0$. Then, the governing equations (2a)–(2d) of motion are reduced to

$$\nabla_0 u - \frac{v^2}{r} - \frac{w^2}{2} \cos\theta = -\frac{\partial p_1}{\partial r} + \Delta_0 u - \frac{u}{r^2} - \frac{2}{r^2} \frac{\partial v}{\partial \theta}, \tag{10a}$$

$$\nabla_0 v + \frac{uv}{r} + \frac{w^2}{2}\sin\theta = -\frac{1}{r}\frac{\partial p_1}{\partial \theta} + \Delta_0 v - \frac{v}{r^2} + \frac{2}{r^2}\frac{\partial u}{\partial \theta}, \tag{10b}$$

$$\nabla_0 w = D\frac{\mathrm{d}f}{\mathrm{d}z} + \Delta_0 w, \qquad \frac{\partial u}{\partial r} + \frac{u}{r} + \frac{1}{r}\frac{\partial v}{\partial \theta} = 0, \tag{10c, d}$$

where $\nabla_0 = \nabla_\delta$ at $\delta = 0$, $\Delta_0 = \Delta_\delta$ at $\delta = 0$, and $D = (2\varepsilon)^{1/2}G = 4(2\varepsilon)^{1/2}\mathrm{Re_s}$ is the Dean number. Here, $\mathrm{Re_s} = G/4$ is the Reynolds number defined with respect to the centerline velocity in a Poiseuille flow. D is regarded as the dynamical similarity parameter for curved pipe flows and is a measure of secondary flow. Now if we introduce the secondary stream function ψ and the vorticity function Ω defined through

$$u = \frac{1}{r}\frac{\partial \psi}{\partial \theta}, \quad v = -\frac{\partial \psi}{\partial r}, \quad \Omega = \frac{\partial v}{\partial r} + \frac{v}{r} - \frac{1}{r}\frac{\partial u}{\partial r}, \tag{11}$$

then the equation of continuity (10d) is identically satisfied and the momentum equations (10a)–(10c) are reduced to

$$\frac{\partial^2 \psi}{\partial r^2} + \frac{1}{r}\frac{\partial \psi}{\partial r} + \frac{1}{r^2}\frac{\partial^2 \psi}{\partial \theta^2} = -\Omega, \tag{12a}$$

$$\frac{\partial^2 \Omega}{\partial r^2} + \frac{1}{r^2}\frac{\partial^2 \Omega}{\partial \theta^2} + 2\mu(r,\theta)\frac{\partial \Omega}{\partial \theta} + 2\lambda(r,\theta)\frac{\partial \Omega}{\partial r} = w\left[\frac{\partial w}{\partial r}\sin\theta + \frac{1}{r}\frac{\partial w}{\partial \theta}\cos\theta\right], \tag{12b}$$

$$\frac{\partial^2 w}{\partial r^2} + \frac{1}{r^2}\frac{\partial^2 w}{\partial \theta^2} + 2\mu(r,\theta)\frac{\partial w}{\partial \theta} + 2\lambda(r,\theta)\frac{\partial w}{\partial r} = -D\frac{\mathrm{d}f}{\mathrm{d}z}, \tag{12c}$$

where

$$\lambda(r,\theta) = \frac{1}{2r}\left(1 - \frac{\partial \psi}{\partial \theta}\right) \quad \text{and} \quad \mu(r,\theta) = \frac{1}{2r}\frac{\partial \psi}{\partial r}. \tag{12d}$$

The boundary conditions (6) and (8) are reduced to

$$w = \psi = \frac{\partial \psi}{\partial r} = 0 \quad \text{at} \quad r = \eta(z) \quad \text{and} \quad r = k, \tag{13a}$$

$$\frac{\partial w}{\partial \theta} = 0, \psi = 0 = \Omega \quad \text{at} \quad \theta = 0 \quad \text{and} \quad \theta = \pi, \tag{13b}$$

$$w(r,-\theta) = w(r,\theta), \quad \psi(r,-\theta) = -\psi(r,\theta), \quad \Omega(r,-\theta) = -\Omega(r,\theta). \tag{13c}$$

As mentioned before, $\mathrm{d}f/\mathrm{d}z$ is an unknown function of z which will be determined by using the constant flux condition given by

$$\frac{(2\varepsilon)^{-1/2}}{\pi}\int_k^{\eta(z)}\int_0^{2\pi} w(r,\theta,z)r\,\mathrm{d}r\,\mathrm{d}\theta = Q(k,D), \tag{14}$$

where $Q(k,D)$ is the flow rate in a curved annulus without constriction. In view of the symmetric condition (13b, c), it is necessary to determine the flow field only within the semi-annular region $k \le r \le \eta(z)$, $0 \le \theta \le \pi$. The simplified equation of motion (12a)–(12d), and the boundary conditions (13a)–(13c) are considered in Collins and Dennis [9]. But, those were for flow in a non-constricted curved pipe with $f(z) = z$. On the contrary, the present problem

deals with the flow in a constricted curved annulus and $f(z)$ is required to be determined using the constant flux condition (14). So, the flow variables will depend on the axial distance z and radii ratio k through the boundary conditions (13a) in addition to their dependence on the Dean number D. In the following section, we present a numerical method for the solution of our problem based on the work of Collins and Dennis [9].

3. Numerical schemes and computational procedure

Let us divide the semi-annular region $[k, \eta(z)] \times [0, \pi]$ into a grid formed by a set of radial lines which cut a set of semi-circular arcs concentric with the boundaries $r = k$ and $r = \eta(z)$. At any fixed axial point z, the grid points are uniformly spaced with spacing h_1 in the direction of r and h_2 in the direction of θ. Since the number of grid points is kept constant irrespective of the axial point z, the mesh size h_1 varies as we go downstream along the length of the annulus (*i.e.*, $h_1 = h_1(z)$). If N_1 and N_2 denote the number of sub-intervals into which the intervals $[k, \eta]$ and $[0, \pi]$ are divided, then the grid spacings h_1 and h_2 in radial and angular directions are given by $h_1 = (\eta(z) - k)/N_1$ and $h_2 = \pi/N_2$. The grid points are given by (r_i, θ_j) in which r_i's and θ_j's are defined by $r_i = k + (i-1)h_1$, $i = 1, \ldots, N_1 + 1$ and $\theta_j = (j-1)h_2$, $j = 1, \ldots, N_2 + 1$. We discretize Equations (12a)–(12c) by using a central-difference formula at each grid point (r_i, θ_j) in the flow domain in a manner similar to that discussed in Collins and Dennis [9]. The discretized version of the stream-function equation (12a) is given by

$$(1 + h_1/2r_i)\psi_{i+1,j} + (1 - h_1/2r_i)\psi_{i-1,j} + (h_1^2/h_2^2 r_i^2)(\psi_{i,j+1} + \psi_{i,j-1}) - 2(1 + h_1^2/h_2^2 r_i^2)\psi_{i,j}$$

$$+ h_1^2 \Omega_{i,j} = 0, i = 2, \ldots, N_1, j = 2, \ldots, N_2. \tag{15}$$

These finite-difference equations are solved subject to the boundary conditions $\psi_{i,1} = 0 = \psi_{i,N2+1}$, $i = 1, \ldots, N_1 + 1$ and $\psi_{1,j} = 0 = \psi_{N_1+1,j}$, $j = 2, \ldots, N_2$. Again, the discretized version of the vorticity transport equation (12b), after rearranging various terms to make the coefficient matrix diagonally dominant, is given by

$$C_1\Omega_{i+1,j} + C_2\Omega_{i,j+1} + C_3\Omega_{i-1,j} + C_4\Omega_{i,j-1} - C_0\Omega_{i,j} - (h_1 w_{i,j}/2)[(w_{i+1,j} - w_{i-1,j})\sin\theta_j$$

$$+ (h_1/h_2 r_i)(w_{i,j+1} - w_{i,j-1})\cos\theta_j] + E_0 = 0, \quad i = 2, \ldots, N_1, \quad j = 2, \ldots, N_2, \tag{16}$$

where the coefficients C_0–C_5 and E_0 are defined in terms of $\lambda_{i,j}$ and $\mu_{i,j}$ by

$$\lambda_{i,j} \geq 0; \quad C_1 = 1 + 2h_1\lambda_{i,j}, \quad C_3 = 1, \tag{17a}$$

$$\lambda_{i,j} < 0; \quad C_1 = 1, \quad C_3 = 1 - 2h_1\lambda_{i,j}, \tag{17b}$$

$$\mu_{i,j} \geq 0; \quad C_2 = (h_1^2/h_2)(1/r_i^2 + 2h_2\mu_{i,j}), \quad C_4 = h_1^2/h_2 r_i^2, \tag{17c}$$

$$\mu_{i,j} < 0; \quad C_2 = h_1^2/h_2^2 r_i^2, \quad C_4 = (h_1^2/h_2^2)(1/r_i^2 - 2h_2\mu_{i,j}), \tag{17d}$$

$$\forall \lambda_{i,j}, \mu_{i,j}; \quad C_0 = 2[1 + h_1|\lambda_{i,j}| + (h_1^2/h_2^2)(1/r_i^2 + h_2|\mu_{i,j}|)], \tag{17e}$$

$$E_0 = -h_1|\lambda_{i,j}|(\Omega_{i+1,j} + \Omega_{i-1,j} - 2\Omega_{i,j}) - (h_1^2|\mu_{i,j}|/h_2)(\Omega_{i,j+1} + \Omega_{i,j-1} - 2\Omega_{i,j}). \tag{17f}$$

The finite-difference equations (16) are solved subject to the boundary conditions $\Omega_{i,1} = 0 = \Omega_{i,N_2+1}$, $i = 1, \ldots, N_1 + 1$ and $\Omega_{1,j} = -2\psi_{2,j}/h_1^2$, $\Omega_{N_1+1,j} = -2\psi_{N_1,j}/h_1^2$, $j = 2, \ldots, N_1$. The vorticity function Ω on the boundaries $r = k$ and $r = \eta(z)$ has been obtained from the stream-function equation (12a) by use of a central-difference formula and boundary condition (13a). Finally, the discretized version of the axial momentum equation (12c), obtained in a manner similar to that of the vorticity transport equation (12b), is given by

$$C_1 w_{i+1,j} + C_2 w_{i,j+1} + C_3 w_{i-1,j} + C_4 w_{i,j-1} - C_0 w_{i,j} + F_0 + h_1^2 D \frac{\mathrm{d}f}{\mathrm{d}z} = 0,$$
$$i = 2, \ldots, N_1, \quad j = 1, \ldots, N_2 + 1, \tag{18}$$

where the coefficients C_0–C_5 are exactly the same as defined in Equations (17a)–(17e) and E_0 is same as the correction term F_0 defined by Equation (17f) but with Ω replaced by w. Since w is also unknown on the boundaries $\theta = 0$ and $\theta = \pi$, the above finite-difference equations include the grid points on these boundaries. The finite-difference equations (18) are solved subject to the boundary conditions $w_{i,j-1} = w_{i,j+1}$, $i = 2, \ldots, N_1$, $j = 1, N_2 + 1$ and $w_{1,j} = 0 = w_{N_1+1,j}$, $j = 1, \ldots, N_2 + 1$.

It is to be noted that, for any fixed value of $\mathrm{d}f/\mathrm{d}z$, if E_0 and F_0 in Equations (16) and (18) are neglected, then the resulting numerical schemes are equivalent to the method of forward and backward difference employed by Greenspan [8] for evaluating the flow field in a non-constricted curved tube. This method has the advantage that the matrices associated with the discretized equations are diagonally dominant, and therefore, these equations are very amenable to solution by an iterative method. However, this method is less accurate than the method in which the correction terms E_0 and F_0 are included, as in the numerical schemes (16) and (18), which makes the schemes accurate to the order of $O(h_1^2, h_2^2)$. Thus, the basic technique involved in the computations is, for any fixed value of $\mathrm{d}f/\mathrm{d}z$, to find solutions of the finite-difference equations (15), (16) and (18) with $E_0 = 0 = F_0$ and then to introduce the corrections E_0 and F_0 through an iterative procedure. This method is similar to that proposed by Dennis and Chang [27] and discussed in detail in Collins and Dennis [9]. Besides, our computations involve another iteration for the unknown function df/dz, which need to be evaluated using the constant flux condition (14). We discuss below only the important points in the computation of solutions for the present problem.

For a fixed value of the radii ratio k, we obtain the solutions for a set of values of Dean number D and axial distance z in increasing order. For each value of D and z, we guess a value of $\mathrm{d}f/\mathrm{d}z$, and obtain the solutions of the finite-difference equations (15), (16) and (18) subject to the appropriate boundary conditions discussed above. Once the solutions are obtained, we compute the flow rate $Q_z(k, D, z)$ by evaluating the double integral in Equation (14) and find the error (ERR = $Q(k, D) - Q_z(k, D, z)$) in the computed flow rate. Depending on the nature of the error (undershoot or overshoot, *i.e.*, ERR is positive or negative), an appropriate increment DPG (positive or negative) to $\mathrm{d}f/\mathrm{d}z$ is given based on the half-interval algorithm in the shooting method (see Chow [28, Chapter 4]). Then the whole computational procedure is repeated. The iteration process is stopped when the error ERR or the increment DPG satisfies some pre-assigned error criteria. At the entrance $z = 0$, we assign $\mathrm{d}f/\mathrm{d}z = 1$ as our initial guess. For a downstream point $z + \delta z$, we assign $\mathrm{d}f/\mathrm{d}z\,(z + \delta z) = \mathrm{d}f/\mathrm{d}z\,(z)$ (the converged value of $\mathrm{d}f/\mathrm{d}z$ at the upstream point z) as our initial guess for a faster convergence of the iteration process for $\mathrm{d}f/\mathrm{d}z$. At $z = 0$, the iteration process converges in one iteration, since the solution at this point corresponds to the solution in a curved annulus without constriction

(*i.e.*, for $\delta_1 = 0$ or $\eta = 1$). We compute the solutions until $z = 0{\cdot}5$, since the solutions at $z = 0{\cdot}5 + \delta z$ are equal to the solutions at $z = 0{\cdot}5 - \delta z$.

For a fixed value of $\mathrm{d}f/\mathrm{d}z$, we obtain first the solutions of the finite difference equations (15), (16) and (18) by considering $E_0 = 0 = F_0$ at each grid point. Then, the associated matrices become diagonally dominant which ensures convergence of the Gauss-Seidel and successive overrelaxation types of iterative methods used for these equations. We compute the solutions of Equations (15), (16) and (18) with the current values of E_0 and F_0 through the following steps.

I. The solution for w is obtained first from Equations (18) by using the solution of ψ at the preceding iteration and the no-slip and symmetric boundary conditions discussed following Equations (18).

II. The computed solution for w is then used in Equations (16) which are subsequently solved for Ω using the derived boundary conditions for Ω discussed following Equations (16). The solution of ψ at the preceding iteration is used to derive the boundary conditions for Ω. Actually the condition for the vorticity Ω at the inner and outer wall, $r = k$ and $r = \eta(z)$, is obtained by employing the following smoothing technique:

$$\Omega_{1,j}^{(m+1)} = -\frac{2\omega\psi_{2,j}^{(m)}}{h_1^2} + (1-\omega)\Omega_{1,j}^{(m)}, \quad \Omega_{N_1+1,j}^{(m+1)} = -\frac{2\omega\psi_{N_1,j}^{(m)}}{h_1^2} + (1-\omega)\Omega_{N_1+1,j}^{(m)}, \quad (19)$$

for $j = 2, \ldots, N_2$, where $0 < \omega \leq 1$ is the smoothing (relaxation) parameter. Thus, the boundary condition for Ω at $r = k$ and $r = \eta(z)$ at $(m+1)$th iteration is obtained using the values of Ω and ψ at the mth iteration. The choice of ω controls the convergence of the iterative procedure in the sense that, if the procedure tends to diverge for a given value of ω, then a reduced value of ω will generally make the procedure convergent.

III. The solution of Ω is then introduced in Equations (15), which are subsequently solved for ψ subject to the boundary conditions discussed following Equations (15). The solution for ψ then provides an updated information for the next iteration.

The above iteration procedure (steps I to III) is repeated until all the solutions approach definite limits subject to a pre-assigned error of tolerance. The criterion for the convergence of the iteration procedure is set as the following L_2 norm:

$$\max_{\mathbf{V}} \left[\sum_{i=1}^{N_1+1} \sum_{j=1}^{N_2+1} (\mathbf{V}_{i,j}^{(m+1)} - \mathbf{V}_{i,j}^{(m)})^2 \right]^{1/2} \leq \mathrm{TOL}, \quad (20)$$

where TOL is some pre-assigned error of tolerance for the solution vector $\mathbf{V} = (w, \Omega, \psi)$. The value of TOL is taken to be 10^{-5}.

Once the solutions of the finite-difference equations (15), (16) and (18) with $E_0 = 0 = F_0$ are obtained, the correction terms E_0 and F_0 are calculated from these solutions at each grid point and are introduced into Equations (16) and (18). Then the above iteration procedure (steps I to III) is repeated until a new solution is approached satisfying the accuracy criterion (20). The corrections terms E_0 and F_0 are then recalculated from this solution and the process is repeated until, eventually, recalculation of E_0 and F_0 does not result in change in the solution to within the accepted accuracy criterion (20).

The convergence of the overall iterative procedure is found to be highly dependent on the initial guess solutions of ψ, Ω and w. So, the solution for different values of Dean number D is obtained in steps from $D = 50$ to $D = 2000$ with an increment $\Delta D = 50$. For $D = 50$,

the solution for a straight annulus is taken as the initial guess solution for the present problem. For other values of D, the final solution for the preceding value of D is taken as the initial guess solution. It is observed that the convergence of the above iterative scheme is very fast for smaller values of D and larger values of k. But, for higher values of D ($D \geq 1000$) and smaller values of k ($k \leq 0{\cdot}2$), the iteration scheme takes more time for computation.

4. Results and discussions

The objective of the present investigation is to study numerically the flow of an incompressible Newtonian fluid in a curved annulus with a local constriction at the outer wall and to apply the results to analyse the flow characteristics in a catheterised curved artery with stenosis for larger values of Dean number D which was the limitation of the analytic approach of Dash *et al.* [25]. Although the results, based on the simplified equations, are restricted to small values of the curvature parameter ε, geometric parameter δ, and constriction parameter δ_1, there is no such restriction on the Dean number D for the results to be valid. For numerical calculations, we fix the parameters ε, δ and δ_1 at 0·1. The case $\delta_1 = 0$ is also considered to study the flow characteristics in a curved annulus of uniform cross-section (*i.e.*, without constriction). The results are obtained for different values of radii ratio $0{\cdot}1 \leq k \leq 0{\cdot}7$ and Dean number $50 \leq D \leq 2000$ based on 11 grid points (*i.e.*, $N_1 = 10$) in radial direction and 19 grid points (*i.e.*, $N_2 = 18$) in the azimuthal direction. Since our primary goal is the application of the model to blood flow in a catheterised stenosed artery, we have not done a grid-independent test of the results. As discussed in Collins and Dennis [9], 11×19 grid points should be enough to obtain the desired accuracy. In our subsequent discussions, the subscript z refers to the axial variation of a variable in the presence of a constriction.

4.1. Flow rate and pressure gradient

The variation of flow rate Q with Dean number D in a curved annulus without constriction (*i.e.*, $\delta_1 = 0$ or $\eta = 1$) for different values of radii ratio k is shown in Figure 3. It is seen that, for a fixed value of D, the flow rate Q decreases with an increase in the value of k. Therefore, this figure describes the reduction in flow rate in a curved annulus compared to that in a curved tube if a constant pressure gradient is maintained in both geometries. It is also observed that, for smaller values of radii ratio k (*e.g.*, for $k < 0{\cdot}4$), the variation of flow rate Q with Dean number D is nonlinear. But, as the value of k increases, the relation between Q and D becomes linear, which is a characteristic of straight tubular/annular flows. Thus, for larger values of k, the effect of curvature on flow rate is almost nullified.

In the presence of constriction, the flux in the constricted curved annulus is fixed at the value $Q(k, D)$ discussed above to obtain the axial variation of pressure gradient G_z, where G_z is defined by

$$G_z = \delta \frac{\partial p}{\partial z} \approx G \frac{\mathrm{d}f}{\mathrm{d}z} = (2\varepsilon)^{-1/2} D \frac{\mathrm{d}f}{\mathrm{d}z}. \tag{21}$$

We refer $\mathrm{d}f/\mathrm{d}z$ as the normalised axial pressure gradient. The axial variation of $\mathrm{d}f/\mathrm{d}z$ for $D = 1000$ and different values of k is shown in Figure 4(A), while the variation of $\mathrm{d}f/\mathrm{d}z$ with k at peak constriction (*i.e.*, at $z = 0{\cdot}5$) for different values of D ($D = 100$ and $D = 2000$) is shown in Figure 4(B). It is seen that $\mathrm{d}f/\mathrm{d}z$ is independent of the radii ratio k at $z = 0$ and $z = 1$. But, as we go along the constricted length, $\mathrm{d}f/\mathrm{d}z$ varies considerably. From the

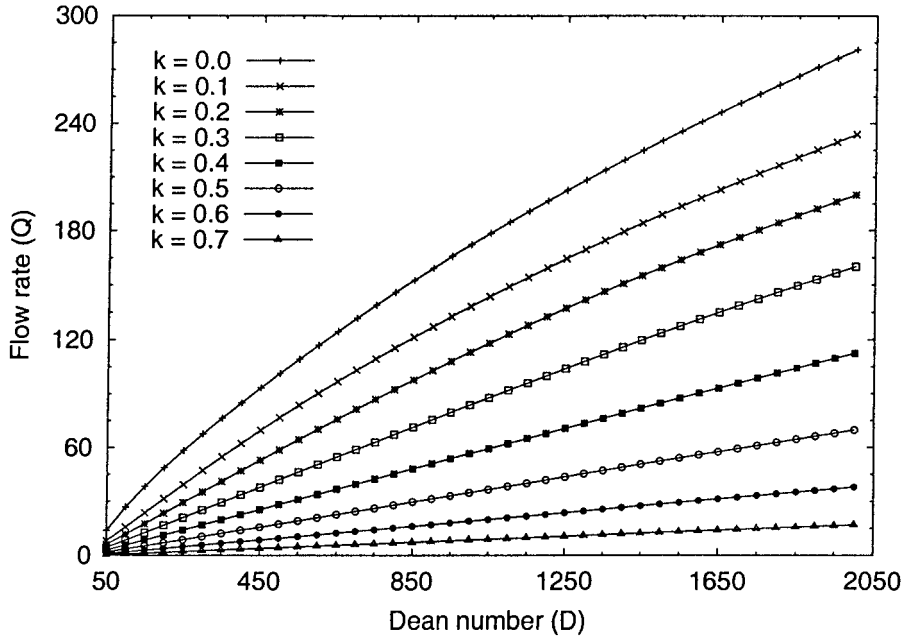

Figure 3. Variation of flow rate Q with Dean number D for constriction parameter $\delta_1 = 0$, curvature parameter $\varepsilon = 0{\cdot}1$, and different values of radii ratio k.

value 1 at $z = 0$, it increases monotonically and takes a maximum value at $z = 0.5$, where the constriction height is also maximum, and then it falls to the value 1 at $z = 1$. In fact, the value $\mathrm{d}f/\mathrm{d}z = 1$ at $z = 0$ and $z = 1$ corresponds to the value in a curved annulus without constriction (*i.e.*, for $\delta_1 = 0$ or $\eta = 1$). With the increase in the value of k, $\mathrm{d}f/\mathrm{d}z$ increases in the constricted region. But, it is almost independent of the value of D, as is seen in Figure 4(B). For larger values of radii ratio k, say $k \geq 0.4$, the normalised pressure gradient $\mathrm{d}f/\mathrm{d}z$ in the constricted curved annulus agrees well with the corresponding result in a constricted straight annulus which is given by

$$\frac{\mathrm{d}f}{\mathrm{d}z} = \frac{\log(k/\eta)[(1-k^4)\log k + (1-k^2)^2]}{\log k[(\eta^4 - k^4)\log(k/\eta) + (\eta^2 - k^2)^2]}. \tag{22}$$

4.2. Pressure drop and frictional resistance

The pressure drop Δp_z and the corresponding frictional resistance FR_z at any point z in the axial direction are given, respectively, by

$$\Delta p_z = \int_0^z G_z \,\mathrm{d}z \approx (2\varepsilon)^{-1/2} D \int_0^z \mathrm{d}f = (2\varepsilon)^{-1/2} D f(z), \tag{23}$$

and

$$FR_z = \frac{1}{z}\frac{\Delta p_z}{Q} \approx (2\varepsilon)^{-1/2}\frac{D}{Q}\frac{f(z)}{z}. \tag{24}$$

The axial variation of pressure drop Δp_z for Dean number $D = 1000$ and different values of radii ratio k is shown in Figure 5(A), whereas the variation of the overall pressure drop

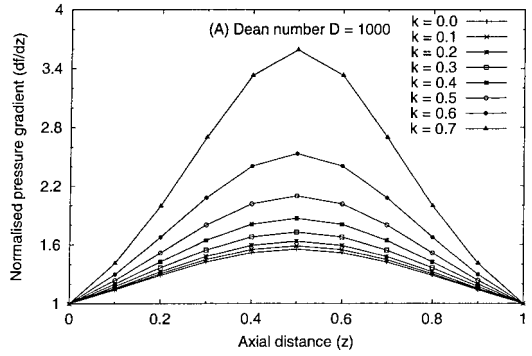

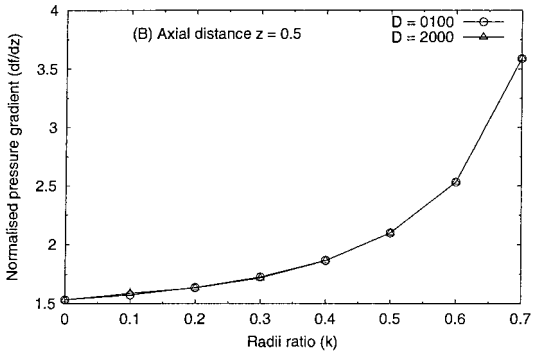

Figure 4. (A) Axial variation of normalised pressure gradient df/dz in the presence of constriction with constricted parameter $\delta_1 = 0{\cdot}1$, curvature parameter $\varepsilon = 0{\cdot}1$, Dean number $D = 1000$, and different values of radii ratio k; (B) Variation of df/dz with k at the peak ($z = 0{\cdot}5$) of constriction for $\delta_1 = 0{\cdot}1$, $\varepsilon = 0{\cdot}1$, and different values of D.

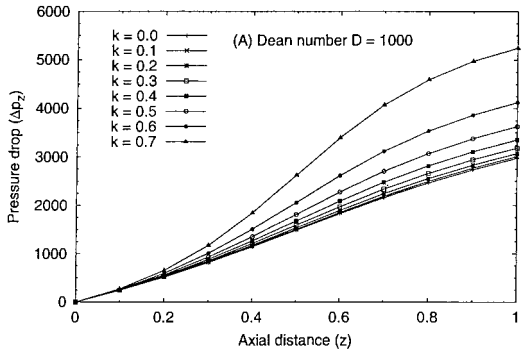

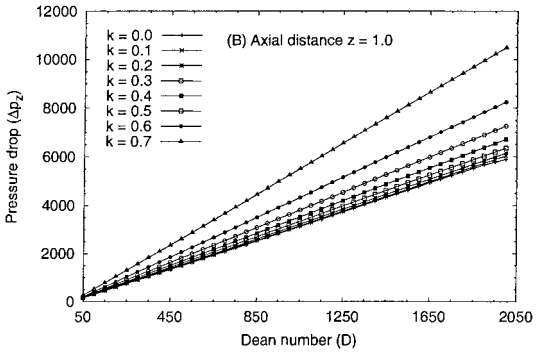

Figure 5. (A) Axial variation of pressure drop Δp_z in the presence of constriction with constricted parameter $\delta_1 = 0{\cdot}1$, curvature parameter $\varepsilon = 0{\cdot}1$, Dean number $D = 1000$, and different values of radii ratio k; (B) Variation of Δp_z with D at the exit ($z = 1$) of constriction for $\delta_1 = 0{\cdot}1$, $\varepsilon = 0{\cdot}1$, and different values of k.

Δp (*i.e.*, Δp_z at $z = 1$ or over the whole constricted length) with the Dean number D for different values of radii ratio k is shown in Figure 5(B). It is seen from Figure 5(A) that, unlike the pressure gradient G_z, the pressure drop Δp_z increases monotonically along the length of the constriction from a minimum value (zero) at $z = 0$ to a maximum value at $z = 1$. Also, the pressure drop Δp_z increases with the increase in the value of radii ratio k and varies considerably across the constricted length for higher values of k. It is observed from Figure 5(B) that the overall pressure drop Δp increases almost linearly with the Dean number D. In the absence of constriction (*i.e.*, for $\delta_1 = 0$ or $\eta = 1$), the pressure drop Δp over a unit length of the annulus is $(2\varepsilon)^{-1/2}D$ which is independent of radii ratio k. But, in the presence of constriction with $\delta_1 = 0{\cdot}1$, the pressure drop Δp over the entire length of the constriction (*i.e.*, Δp_z at $z = 1$) increases with the increase in radii ratio k.

The axial variation of frictional resistance FR_z for $D = 1000$ and different values of k is shown in Figure 6(A), while the variation of frictional resistance FR_z with the radii ratio k at the entrance ($z = 0$) and exit ($z = 1$) of the constriction for different values of Dean number D ($D = 100$ and $D = 2000$) is shown in Figure 6(B). The frictional resistance FR in a curved annulus without constriction (*i.e.*, for $\delta_1 = 0$ or $\eta = 1$) corresponds to the value

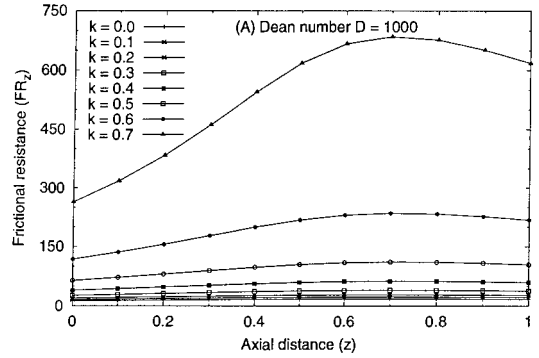

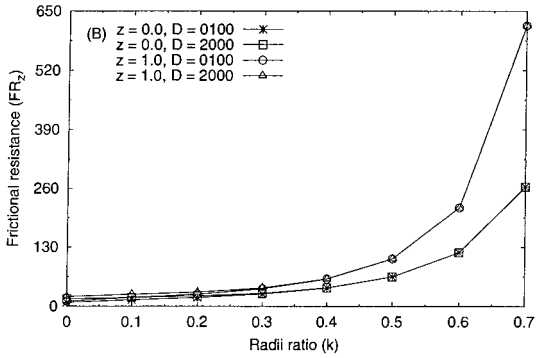

Figure 6. (A) Axial variation of frictional resistance FR_z in the presence of constriction with constricted parameter $\delta_1 = 0{\cdot}1$, curvature parameter $\varepsilon = 0{\cdot}1$, Dean number $D = 1000$, and different values of radii ratio k; (B) Variation of FR_z with k at the entrance ($z = 0$) and exit ($z = 1$) of constriction for $\delta_1 = 0{\cdot}1$, $\varepsilon = 0{\cdot}1$, and different values of D.

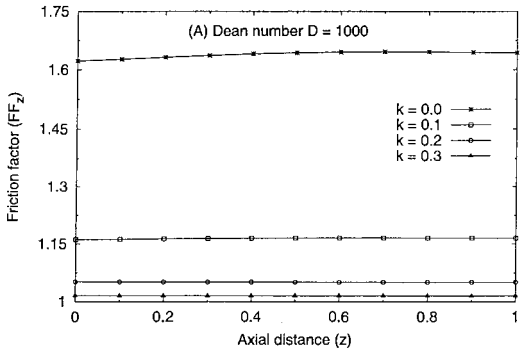

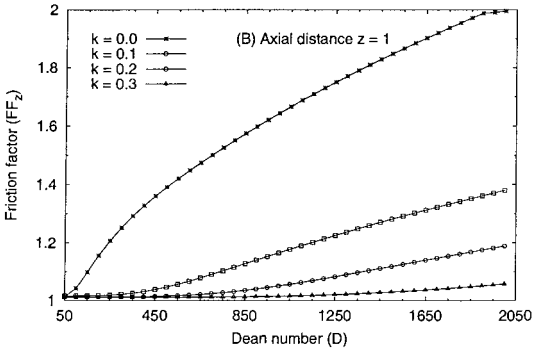

Figure 7. (A) Axial variation of friction factor FF_z in the presence of constriction with constricted parameter $\delta_1 = 0{\cdot}1$, curvature parameter $\varepsilon = 0{\cdot}1$, Dean number $D = 1000$, and different values of radii ratio k; (B) Variation of FF_z with D at the exit ($z = 1$) of constriction for $\delta_1 = 0{\cdot}1$, $\varepsilon = 0{\cdot}1$, and different values of D.

of FR_z at $z = 0$. It is seen from Figure 6(A) that the frictional resistance FR_z in a constricted curved tube (*i.e.*, for $k = 0$) does not vary much over the length of the constriction. But, in a constricted curved annulus with relatively higher value of radii ratio k, it varies significantly over the length of the constriction. It is further depicted that the frictional resistance FR_z in the downstream of the constriction is higher than the corresponding value in the upstream. It is observed from Figure 6(B) that the frictional resistance FR_z does not vary much with the Dean number D, and it becomes almost independent of D (*i.e.*, the effect of curvature is nullified) for higher values of radii ratio k (*e.g.*, for $k \geq 0.4$). It is further depicted that, for higher values of k, the frictional resistance in the presence of a constriction (*i.e.*, FR_z at $z = 1$) is considerably higher than the corresponding value in the absence of a constriction (*i.e.*, FR_z at $z = 0$). However, the frictional resistance FR_z increases with the increase in the value of radii ratio k.

4.3. Application to a catheterised artery

The insertion of a catheter into an artery leads to the formation of an annular region between the catheter wall and the arterial wall. Therefore, the flow characteristics in an annulus will have significant applications in understanding the changed flow pattern in an artery in the presence of a catheter and deducing the catheter induced effects on various physiologically important flow characteristics (see Back [29], Back *et al.* [30], and Dash *et al.* [25]).

It can be inferred from our present results that the insertion of a catheter into an artery leads to an increase in the frictional resistance. The factor by which frictional resistance increases due to catheterisation can be estimated by obtaining the ratio of frictional resistance in a catheterised artery to that in an uncatheterised artery. In the presence of stenosis (*i.e.*, constriction), this frictional resistance ratio FRR_z at any axial point z is given by

$$FRR_z^{cc} = \frac{FR_z^{cc}}{FR_z^{cu}} \approx \frac{Q(0, D)}{Q(k, D)} \frac{f(k, D, z)}{f(0, D, z)}, \tag{25}$$

where the superscripts cc and cu refer to a 'curved catheterised' and 'curved uncatheterised' artery, respectively. In the absence of curvature (*i.e.*, for $\varepsilon = 0$), the expression for FRR_z can be written as

$$FRR_z^{sc} = \frac{FR_z^{sc}}{FR_z^{su}} = \frac{\log K}{(1 - K^4) \log K - (1 - K^2)^2}, \tag{26}$$

where $K = k/\eta(z)$ and the superscripts sc and su refer to a 'straight catheterised' and 'straight uncatheterised' artery, respectively. Thus, the frictional resistance ratio FRR_z in a straight catheterised artery is a function of only catheter radius k and axial distance z. In a curved catheterised artery, it depends on Dean number D in addition to k and z. In the absence of stenosis (*i.e.*, for $\delta_1 = 0$ or $\eta = 1$), the frictional resistance ratios FRR^{cc} and FRR^{sc} correspond to the values of FRR_z^{cc} and FRR_z^{sc} at $z = 0$, respectively.

The comparison of frictional resistance ratio FRR in a curved catheterised artery ($\varepsilon = 0{\cdot}1$) with that in a straight catheterised artery ($\varepsilon = 0$) corresponding to $\delta_1 = 0$ (without stenosis) and $\delta_1 = 0{\cdot}1$ (with stenosis) and different values of k and D are shown in Tables 1 and 2, respectively. It is observed that the frictional resistance ratio FRR increases with the increase in the value of radii ratio k. Again, in a curved catheterised artery, FRR is smaller than the corresponding value in a straight catheterised artery, and it decreases further with the increase in Dean number D. Thus, these results indicate that the increase in the frictional resistance (or equivalently, the increase in the pressure gradient at a constant flow rate) due to catheterisation at a higher value of D is less than that at a lower value of D. For $k = 0{\cdot}5$, the frictional resistance in the catheterised artery without stenosis (*i.e.*, for $\delta_1 = 0$ or $\eta = 1$) is about 5·8 times of the value in the uncatheterised artery at $D = 500$ and 4 times the value in the uncatheterised artery at $D = 2000$. In the presence of stenosis with $\delta_1 = 0{\cdot}1$, this increase factor (7·2 at $D = 500$ and 4·97 at $D = 2000$) is even higher than the corresponding value in the absence of stenosis for which $\delta_1 = 0$ or $\eta = 1$.

4.4. Calculation of friction factor

In studies of flow characteristics in curved tubes/annulus, it is often desired to estimate the friction factor (ratio of frictional resistance in a curved tube/annulus to that in a straight tube/annulus). It describes precisely the effect of curvature on the flow characteristics. In the presence of a constriction, it is given by

Table 1. Frictional resistance ratio FRR in a straight ($\varepsilon = 0$) and curved (ε = 0·1) catheterised artery without stenosis ($\delta_1 = 0$) (*i.e.*, FRR_z at $z = 0$) for different values of catheter radius k and Dean number D.

k/D	$\varepsilon = 0, \delta_1 = 0$	ε = 0·1, $\delta_1 = 0$				
	for all Re	$D = 100$	$D = 500$	$D = 1000$	$D = 1500$	$D = 2000$
0·1	1·741	1·705	1·323	1·246	1·220	1·202
0·2	2·349	2·289	1·732	1·523	1·445	1·406
0·3	3·289	3·201	2·414	2·059	1·865	1·756
0·4	4·894	4·760	3·590	3·049	2·723	2·499
0·5	7·938	7·719	5·821	4·943	4·408	4·033
0·6	14·586	14·182	10·695	9·082	8·099	7·409
0·7	32·611	31·709	23·910	20·304	18·105	16·563

Table 2. Frictional resistance ratio FRR in a straight ($\varepsilon = 0$) and curved (ε = 0·1) catheterised artery with stenosis (ε_1 = 0·1) (*i.e.*, FRR_z at $z = 1$) for different values of catheter radius k and Dean number D.

k/D	$\varepsilon = 0, \delta_1$ = 0·1	ε = 0·1, δ_1 = 0·1				
	for all Re	$D = 100$	$D = 500$	$D = 1000$	$D = 1500$	$D = 2000$
0·1	1·779	1·734	1·339	1·261	1·233	1·230
0·2	2·461	2·389	1·797	1·574	1·489	1·466
0·3	3·571	3·463	2·596	2·206	1·990	1·893
0·4	5·596	5·424	4·066	3·442	3·066	2·845
0·5	9·815	9·511	7·189	6·034	5·368	4·970
0·6	20·491	19·854	14·882	12·596	11·206	10·373
0·7	58·266	56·452	42·315	35·813	31·862	29·495

$$FF_z = \frac{FF_z^{\mathrm{ca}}}{FF_z^{\mathrm{sa}}}, \tag{27}$$

where the superscripts ca and sa refer to a 'curved annulus' and 'straight annulus', respectively. In the absence of constriction (*i.e.*, for $\delta_1 = 0$ or $\eta = 1$), FF_z is reduced to

$$FF = \frac{FR^{\mathrm{ca}}}{FR^{\mathrm{sa}}} = \frac{Q^{\mathrm{sa}}}{Q^{\mathrm{ca}}} = \left(\frac{D}{8}\frac{(1-k^4)\log k + (1-k^2)^2}{\log k}\right) \Big/ \left(\frac{1}{\pi}\int_0^{2\pi}\int_k^1 w(r,\theta) r \, \mathrm{d}r \, \mathrm{d}\theta\right). \tag{28}$$

The axial variation of friction factor FF_z for Dean number $D = 1000$ and different values of radii ratio k is shown in Figure 7(A), where as the variation of the overall friction factor FF (*i.e.*, FF_z at $z = 1$ or over the whole constricted length) with the Dean number D for different values of radii ratio k is shown in Figure 7(B). It is seen from these figures that the friction factor FF_z does not vary significantly along the length of the constriction. So, Equation (27) matches with Equation (28) at all axial points z. The friction factor FF in a curved tube (*i.e.*, for $k = 0$), is considerably higher than the corresponding value in a curved annulus. For

$D = 2000$, the friction factor FF in a curved tube (*i.e.*, for $k = 0$) is about 2 (implying a 50% reduction in flow rate due to curvature effect). But, for the same value of D, the friction factor FF in a curved annulus with the value $k = 0{\cdot}1$ is about 1·35 (implying a 26% reduction in flow rate due to curvature effect). For higher values of k, the friction factor decreases further, and for $k \geq 0{\cdot}4$, it becomes almost independent of Dean number D, implying that the curvature effect is almost nullified for $k \geq 0{\cdot}4$. It is further depicted that, for all values of $k \geq 0{\cdot}1$, the variation of friction factor FF with the Dean number D is insignificant compared to that in a curved tube (*i.e.*, for $k = 0$) whenever $D \leq 500$.

4.5. WALL SHEAR STRESS

The non-dimensional wall shear stress (shear stress non-dimensionalised with respect to $\rho(\mu/\rho a)^2$) at any axial point z is approximated by

$$\tau_z \approx -(2\varepsilon)^{-1/2} \left.\frac{\partial w}{\partial r}\right|_{r=1}. \tag{29}$$

It is evaluated numerically by use of a four-point backward-difference formula. The axial variation of wall shear stress τ_z for $D = 1000$, $D = 2000$ and different values of radii ratio k is shown in Figures 8(A,B), whereas the variation of wall shear stress τ_z with the Dean number D at the entrance ($z = 0$) and peak ($z = 0{\cdot}5$) of the constriction for different values of radii ratio k is shown in Figures 8(C,D). The wall shear stress τ in a curved annulus without constriction (*i.e.*, for $\delta_1 = 0$ or $\eta = 1$) corresponds to the value of τ_z at $z = 0$ or $z = 1$. It is seen from Figures 8(A,B) that, for smaller values of radii ratio k, the wall shear stress τ_z varies markedly along the length of the constriction. It is further depicted that the wall shear stress τ_z increases with the increase in Dean number D but decreases with the increase in radii ratio k. For a fixed pressure gradient G, or equivalently for a fixed value of D, an increase in the value of k results in a decrease in flow rate Q (as depicted in Figure 3), which in fact results in a decrease in wall shear stress τ_z But, if the flow rate Q is maintained constant (independent of k), then an increase in the value of k would result in an increase in the pressure gradient G which would, in fact, lead to an increase in the wall shear stress τ_z. It is seen from Figures 8(A,B) that the wall shear stress τ_z remains positive over the entire constricted length. Thus, this analysis could not detect the point of separation in the downstream flow field. To capture the separation points, the governing equations have to include all the ignored terms, and a better numerical procedure has to be used.

4.6. FLOW BEHAVIOUR

Figure 9 shows the secondary streamlines (ψ = constant) in the r-θ plane of a curved annulus without constriction (*i.e.*, for $\delta_1 = 0$ or $\eta = 1$) for (a) $k = 0{\cdot}1$, $D = 1000$, (b) $k = 0{\cdot}1$, $D = 2000$, (c) $k = 0{\cdot}3$, $D = 1000$, (d) $k = 0{\cdot}3$, $D = 2000$, (e) $k = 0{\cdot}5$, $D = 1000$, and (f) $k = 0{\cdot}5$, $D = 2000$. It is observed that the streamline pattern divides each half of the cross-sectional plane into two parts forming two loops, which is in contrast to the streamlines pattern in a curved tube where only one loop formation occurs, unless a dual solution exists (McConalogue and Srivastava [6], Greenspan [8], Collins and Dennis [9], Pedley [3], and Berger *et al.* [4]). The loop near the inner wall is smaller for lower values of radii ratio k. But, as the value of radii ratio k increases, the loop near the inner wall becomes larger and the loop near the outer wall becomes smaller.

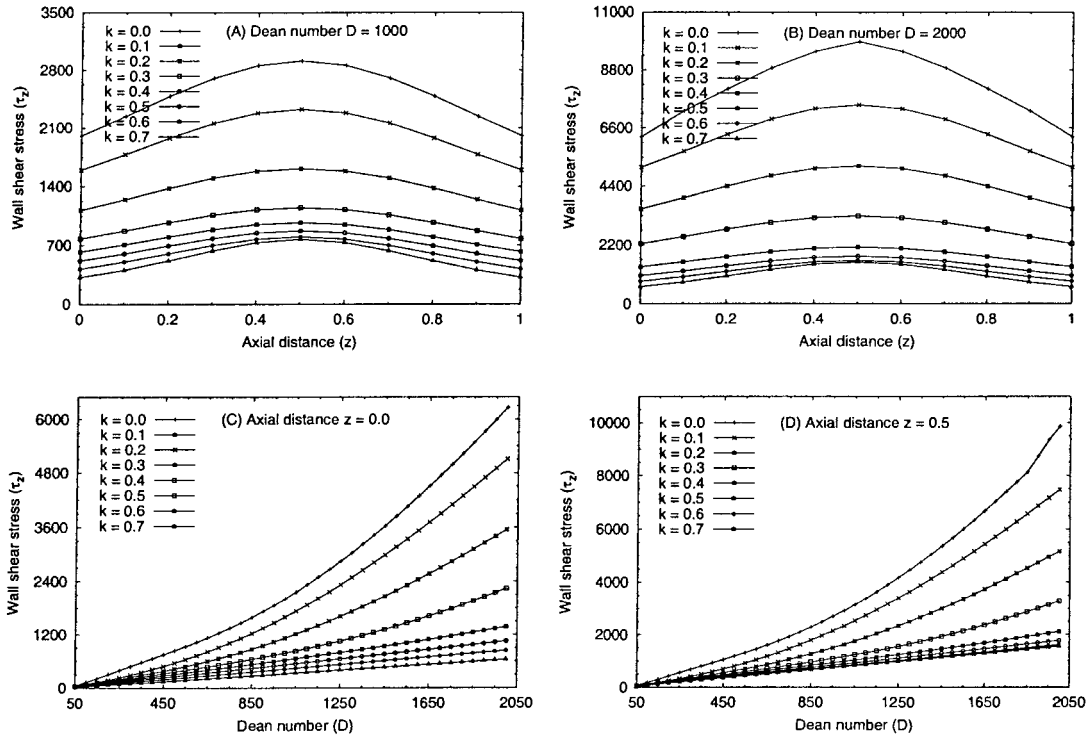

Figure 8. (A,B) Axial variation of wall shear stress τ_z in the presence of constriction with constricted parameter $\delta_1 = 0{\cdot}1$, curvature parameter $\varepsilon = 0{\cdot}1$, Dean number $D = 1000$ and $S = 2000$, and different values of radii ratio k; (C,D) Variation of τ_z with D at the entrance ($z = 0$) and peak ($z = 0{\cdot}5$) of constriction for $\delta_1 = 0{\cdot}1$, $\varepsilon = 0{\cdot}1$, and different values of k.

Figure 10 shows the axial velocity contours (w = constant) in r-θ plane of a curved annulus without constriction (*i.e.*, for $\delta_1 = 0$ or $\eta = 1$) for (a) $k = 0{\cdot}1$, $D = 1000$, (b) $k = 0{\cdot}1$, $D = 2000$, (c) $k = 0{\cdot}3$, $D = 1000$, (d) $k = 0{\cdot}3$, $D = 2000$, (e) $k = 0{\cdot}5$, $D = 1000$, and (f) $k = 0{\cdot}5$, $D = 2000$. It is depicted that, for smaller values of radii ratio k (as depicted for $k = 0{\cdot}1$ and $k = 0{\cdot}3$), the contours form a loop about the point of maximum velocity, which occurs on the axis of symmetry at the outer bend ($\theta = 0°$). As the value of Dean number D increases, the location of maximum velocity is shifted towards the outer wall along the radial line $\theta = 0°$. For larger values of radii ratio k (*e.g.*, for $k \geq 0{\cdot}4$), the location of maximum of velocity does not vary with Dean number D; in fact, the axial velocity w does not vary much with the azimuthal angle θ which is a characteristic of straight tubular/annular flow. The line joining the points of equal velocity in the cross-sectional plane becomes parallel to the inner and outer wall as depicted in Figures 10(e,f) for $k = 0{\cdot}5$.

5. Conclusions

The present numerical investigation on flow through a curved annulus with a local constriction at the outer wall brings out many interesting fluid mechanical phenomena due to the effect of flow geometry (inner wall radius, outer wall variation and curvature) as well as the dynamics of flow governed by the Dean number D (dynamical similarity parameter). The results are valid for all values of D corresponding to the entire laminar flow regime. In the annular region,

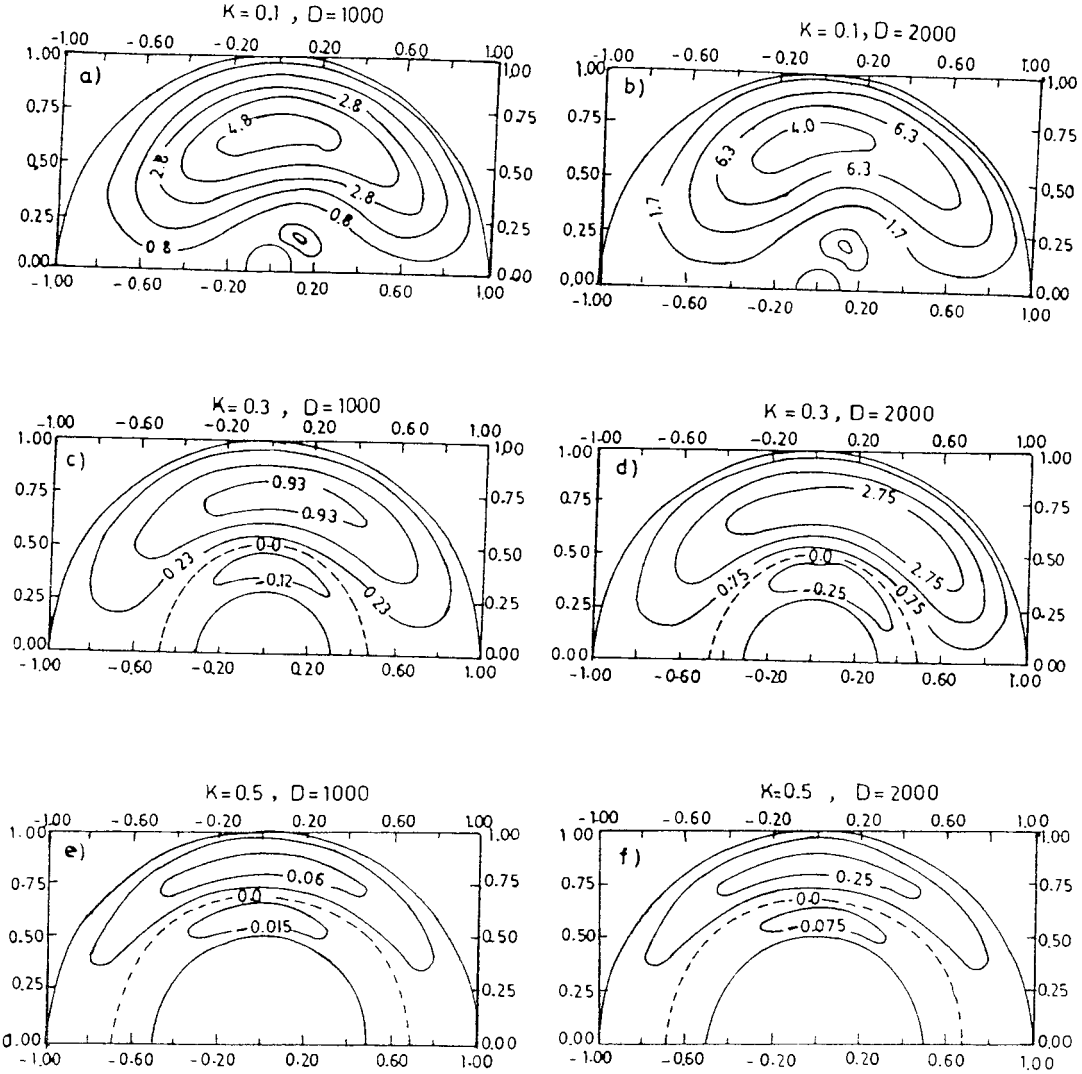

Figure 9. Secondary streamlines (ψ = constant) in r-θ plane in the absence of constriction ($\delta_1 = 0$) for $\varepsilon = 0{\cdot}1$; (a) $k = 0{\cdot}1$, $D = 1000$; (b) $k = 0{\cdot}1$, $D = 2000$; (c) $k = 0{\cdot}3$, $D = 1000$; (d) $k = 0{\cdot}3$, $D = 2000$; (e) $k = 0{\cdot}5$, $D = 1000$; (f) $k = 0{\cdot}5$, $D = 2000$.

the secondary streamlines divide each half of the cross-sectional plane into two parts forming two loops, which implies the formation of an increased number of secondary vortices. For larger values of radii ratio k (*e.g.*, for $k \geq 0{\cdot}4$), the axial velocity contours in a cross-sectional plane become parallel to the walls of the annulus, which in fact indicates that the effect of curvature becomes insignificant as the value of k increases.

The numerical results show that the pressure gradient, pressure drop and frictional resistance vary markedly across the constricted region. Again, an increase in the value of the radii ratio k leads to a considerable increase in their magnitudes. These results are used to estimate the increase in pressure drop or frictional resistance in an artery when a catheter is inserted into it. It is found that, because of the curvature, the increase in frictional resistance due to catheterisation depends on the catheter size (radii ratio k) as well as the Dean number D. In

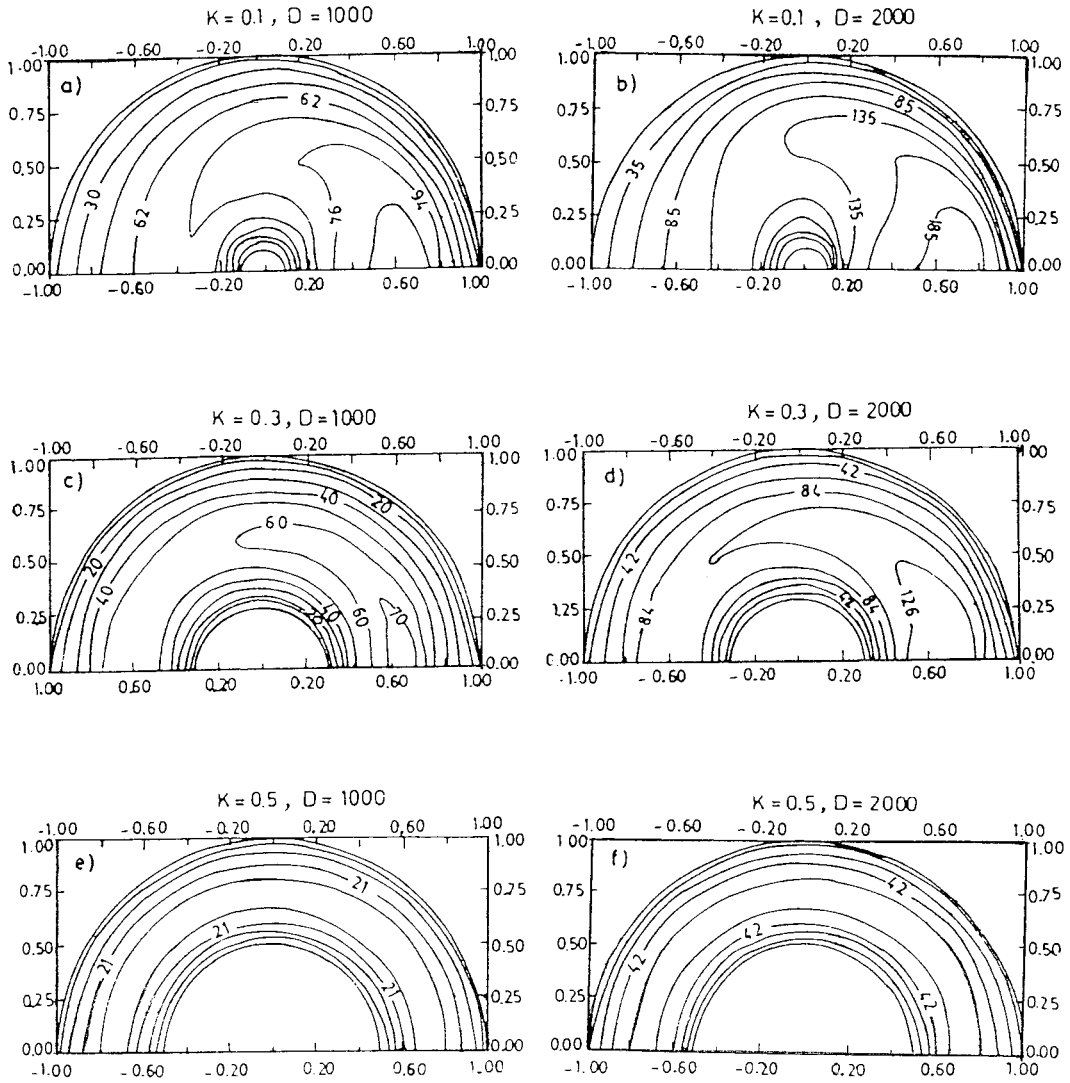

Figure 10. Axial velocity contours (w = constant) in r-θ plane in the absence of constriction ($\delta_1 = 0$) for $\varepsilon = 0{\cdot}1$; (a) $k = 0{\cdot}1$, $D = 1000$; (b) $k = 0{\cdot}1$, $D = 2000$; (c) $k = 0{\cdot}3$, $D = 1000$; (d) $k = 0{\cdot}3$, $D = 2000$; (e) $k = 0{\cdot}5$, $D = 1000$; (f) $k = 0{\cdot}5$, $D = 2000$.

the absence of constriction (*i.e.*, for $\delta_1 = 0$ or $\eta = 1$) and depending on the value of k ranging from 0·1 to 0·7, the frictional resistance increases by a factor ranging from 1·32 to 23·91 for $D = 500$ and 1·20 to 16·56 for $D = 2000$. But, in the presence of constriction with $\delta_1 = 0{\cdot}1$ and with the same range for k, the increase in frictional resistance is by a factor ranging from 1·34 to 42·32 for $D = 500$ and 1·18 to 29·5 for $D = 2000$. In a straight catheterised artery, these increased factors are about 1·74 to 32·61 for $\delta_1 = 0$ and 1·78 to 58·27 for $\delta_1 = 0{\cdot}1$ (for all values of Dean number D). These estimates for the increased frictional resistance can be used to correct the error involved in the measured pressure gradients using catheters.

Table 3. Nomenclature.

Alphabetical symbols	
a	undisturbed radius of the constricted curved (outer) pipe
b	radius of curvature of the curved annulus
d	distance from the origin to the inlet of constriction
D	Dean number
FF	friction factor
FR	frictional resistance
FRR	frictional resistance ratio
G	axial pressure gradient
h	amplitude of the constricted segment
h_1	grid spacing in the radial direction r
h_2	grid spacing in the azimuthal direction θ
H	expression $1 + \varepsilon r \cos\theta$
k	radii ratio (ratio of catheter size to vessel size)
K	ratio of radii ratio to wall variation $(k/\eta(z))$
L	length of the constricted segment
N_1	number of sub-intervals into which the interval $[k, \eta]$ is divided
N_2	number of sub-intervals into which the interval $[0, \pi]$ is divided
p	pressure field
q	velocity field (u, v, w) in (r, θ, z) co-ordinate
Q	flow rate
r	radial distance/co-ordinate
Re	Reynolds number
$\mathrm{Re_s}$	Reynolds number defined with respect to centreline velocity in a Poiseuille flow
U_0	characteristics velocity (defined by $U_0 = \mu/\rho a$)
z	axial distance/co-ordinate
Greek symbols	
δ	geometric parameter (a/L)
δ_1	stenotic parameter (a/h)
ε	curvature parameter (a/b)
$\eta(z)$	variation of the outer wall in the constricted region
φ	toroidal co-ordinate for the axial distance z in a curved tube $(z = b\varphi)$
μ	dynamic viscosity of the fluid/blood
Ω	vorticity function in r-θ plane
ρ	density of the fluid/blood
ψ	stream function in r-θ plane
τ	shear stress at the wall
θ	azimuthal co-ordinate
Subscripts	
z	axial variation of a flow variable in the presence of constriction
Superscripts	
ca	value in a curved annulus (used for FR and Q)
cc	value in a curved catheterised artery (used for FR)
cu	value in a curved uncatheterised artery (used for FR)
sa	value in a straight annulus (used for FR and Q)
sc	value in a straight catheterised artery (used for FR)
su	value in a straight uncatheterised artery (used for FR)

Acknowledgement

The authors are grateful to one of the referees for emphasising the point that the flow rate needs to be maintained constant at each cross section, which brought out a significant improvement in the paper.

References

1. W.R. Dean, Note on the motion of fluid in a curved pipe. *Phil. Mag. J. Sci.* 4 (1927) 208–223.
2. W.R. Dean, The streamline motion of fluid in a curved pipe. *Phil. Mag. Jour. Sci.* 5 (1928) 673–693.
3. T.J. Pedley, *The Fluid Mechanics of Large Blood Vessels*. London: Cambridge University Press (1980) 446 pp.
4. S.A. Berger, L. Talbot and L.S. Yao, Flow in curved pipes. *Ann. Rev. Fluid Mech.* 15 (1983) 461–512.
5. H. Ito, Flow in curved pipes. *JSME Int. J.* II 30 (1987) 543–552.
6. D.J. McConalogue and R.S. Srivastava, Motion of fluid in a curved tube. *Proc. R. Soc. London* A 307 (1968) 37–53.
7. L.C. Truesdell and R.J. Adler, Numerical treatment of fully developed laminar flow in helically coiled tubes. *AIChE J.* 16 (1970) 1010–1015.
8. A.D. Greenspan, Secondary flow in a curved tube. *J. Fluid Mech.* 57 (1973) 167–176.
9. W.M. Collins and S.C.R. Dennis, The steady motion of a viscous fluid in a curved tube. *Q. J. Mech. Appl. Math.* 28 (1975) 133–156.
10. S.C.R. Dennis, Calculation of the steady flow through a curved tube using a new finite-difference method. *J. Fluid Mech.* 99 (1980) 449–467.
11. S.C.R. Dennis and M. Ng, Dual solutions for steady laminar flow through a curved tube. *Q. J. Mech. Appl. Math.* 35 (1982) 305–324.
12. P. Daskopoulos and A.M. Lenhoff, Flow in curved ducts: bifurcation structure for stationary ducts. *J. Fluid Mech.* 203 (1989) 125–148.
13. H.C. Kao, Some aspects of bifurcation structure of laminar flow in curved ducts. *J. Fluid Mech.* 243 (1992) 519–539.
14. P.A.J. Mees, K. Nandakumar and J.H. Masliyah, Instability and transitions of flow in a curved squire duct: the development of two pairs of Dean vortices. *J. Fluid Mech.* 314 (1996) 227–246.
15. N. Padmanabhan and G. Jayaraman, Flow in a curved tube with constriction - an application to the arterial system. *Med. & Biol. Engng. & Compt.* 22 (1984) 216–224.
16. R. Jain and G. Jayaraman, On the steady laminar flow in a curved pipe of varying elliptic cross-section. *Fluid Dyn. Res.* 5 (1990) 351–362.
17. H. Niimi, Y. Kawano and I. Sugiyama, Structure of blood flow through a curved vessel with an aneurysm. *Biorheology* 21 (1984) 603–615.
18. L.J. Chang and J.M. Tarbell, Numerical simulation of fully-developed sinusoidal and pulsatile (physiological) flow in curved tubes. *J. Fluid Mech.* 161 (1985) 175–198.
19. L.J. Chang and J.M. Tarbell, A numerical study of flow in curved tubes simulating coronary arteries. *J. Biomech.* 21 (1988) 927–937.
20. S. Schilt, J.E. Moore Jr., A. Delfino and J.J. Meister, The effects of time-varying curvature on velocity profile in a model of the coronary arteries. *J. Biomech.* 29 (1996) 469–474.
21. A. Sarkar and G. Jayaraman, Correction to flow rate - pressure drop relation in coronary angioplasty: steady streaming effect. *J. Biomech.* 31 (1998) 781–791.
22. M.A. Ebadian, Rate of flow in a concentric pipe of circular cross-section. *J. Appl. Mech., Trans. ASME 57* (1990) 1073–1076.
23. G.T. Karahalios, Some possible effects of a catheter on the arterial wall. *Med. Phys.* 17 (1990) 922–925.
24. G. Jayaraman and K. Tiwari, Flow in a catheterised curved artery. *Med. Biol. Engng. Compt.* 33 (1995) 1–6.
25. R.K. Dash, G. Jayaraman and K.N. Mehta, Flow in a catheterised curved artery with stenosis. *J. Biomech.* 32 (1999) 49–61.
26. D.F. Young, Effect of a time dependent stenosis on flow through a tube. *J. Engng. Ind., Trans. ASME 90* (1968), 248–260.

27. S.C.R. Dennis and G.Z. Chang, Numerical integration of the Navier-Stokes equations for steady two-dimensional flow. *Phys. Fluids Suppl.* II 12 (1969) 88–93.
28. C.Y. Chow, *An Introduction to Computational Fluid Dynamics*. New York: John Wiley and Sons, (1979) 396 pp.
29. L.H. Back, Estimated mean flow resistance increase during coronary artery catheterization. *J. Biomech.* 27 (1994) 169–175.
30. L.H. Back, E.Y. Kwack and M.R. Back, Flow rate-pressure drop relation in coronary angioplasty: catheter obstruction effect. *J. Biomech. Engng., Trans. ASME* 118 (1996) 83–89.